

Thermal evolution of the primordial clouds in warm dark matter models with keV sterile neutrinos

Jaroslaw Stasielak^{1,2,3}, Peter L. Biermann^{2,3,4}, and Alexander Kusenko⁵

ABSTRACT

We analyze the processes relevant for star formation in a model with dark matter in the form of sterile neutrinos. Sterile neutrino decays produce an x-ray background radiation that has a two-fold effect on the collapsing clouds of hydrogen. First, the x-rays ionize the gas and cause an increase in the fraction of molecular hydrogen, which makes it easier for the gas to cool and to form stars. Second, the same x-rays deposit a certain amount of heat, which could, in principle, thwart the cooling of gas. We find that, in all the cases we have examined, the overall effect of sterile dark matter is to facilitate the cooling of gas. Hence, we conclude that dark matter in the form of sterile neutrinos can help the early collapse of gas clouds and the subsequent star formation.

Subject headings: dark matter, neutrinos, reionization, star formation

1. Introduction

Numerous observations, from galaxy rotation curves to gravitational lensing, to cosmic microwave background radiation, all point to the existence of dark matter which is not made of ordinary atoms, but, rather, of some new, yet undiscovered particles. In particular, the abundance of dark matter has been precisely determined recently by the WMAP (Spergel et al. 2003, 2006). However, the nature of dark-matter particles remains unknown. One attractive candidate is a sterile neutrino with mass of several keV and a small mixing with the ordinary neutrinos. If such a particle exists, it could be produced in the early universe with

¹Institute of Physics, Jagiellonian University, ul. Reymonta 4, 30-059 Kraków, Poland

²Max-Planck Institute for Radioastronomy, Bonn, D-53121, Germany

³Department of Physics and Astronomy, University of Bonn, D-53121, Germany

⁴Department of Physics and Astronomy, University of Alabama, Tuscaloosa, AL 35487, USA

⁵Department of Physics and Astronomy, University of California, Los Angeles, CA 90095-1547, USA

the right abundance to be dark matter either from neutrino oscillations (Dodelson & Widrow 1994; Shi & Fuller 1999; Abazajian, Fuller & Patel 2001; Abazajian, Fuller & Tucker 2001; Abazajian 2006a; Dolgov & Hansen 2002), or from some other processes, for example from inflaton decay (Shaposhnikov & Tkachev 2006). The same particle can explain the observed velocities of pulsars because its emission from a cooling neutron star would be anisotropic, hence providing the neutron star with a recoil velocity of a sufficient magnitude (Kusenko & Segrè 1997, 1999; Kusenko, Segrè & Vilenkin 1998; Fuller et al. 2003; Barkovich, D’Olivo & Montemayor 2004, 2005; Kusenko 2004). In addition, the neutrino kick can enhance the convection during the first second of the supernova explosion, which can increase the energy of the supernova shock and bring the supernova calculations in better agreement with the observations (Fryer & Kusenko 2006). Sterile neutrinos can also help the formation of supermassive black holes in the early universe (Munyanza & Biermann 2005; Fan et al. 2001).

Although the dark-matter sterile neutrinos have interactions that are too weak to be discovered in the laboratory, some other sterile neutrinos may exist. Most models of neutrino masses introduce sterile (or right-handed) neutrinos to generate masses of the ordinary neutrinos via the seesaw mechanism (Gell-Mann et al. 1979; Yanagida 1980; Mohapatra & Senjanović 1980). The name *sterile* was coined by Pontecorvo (1967). Many seesaw models assume that sterile neutrinos have very large masses, which makes them unobservable. However, a number of theoretical models predict the existence of sterile neutrinos at or below the electroweak scale (Farzan et al. 2001; Appelquist & Shrock 2002; Asaka & Shaposhnikov 2005; de Gouvêa 2005). There is an indication that some light sterile mass eigenstates may cause the neutrino flavor transformation seen in the Los Alamos Liquid Scintillator Neutrino Detector (LSND) experiment (Athanasopoulos et al. 1998; Sorel, Conrad & Shaevitz 2004; de Gouvêa 2005). The results of LSND are being tested by the MiniBooNE experiment. One can expect that there are at least three light sterile neutrinos (Asaka, Blanchet & Shaposhnikov 2005), in which case the neutrino oscillations can explain the baryon asymmetry of the universe (Akhmedov, Rubakov & Smirnov 1998; Asaka & Shaposhnikov 2005).

Although dark-matter sterile neutrinos are stable on cosmological time scales, they nevertheless decay. The mass matrix is assumed to have the seesaw form with the Majorana mass term of the order of several keV and with a much smaller Dirac mass term. The diagonalization of such a mass matrix yields the light mostly active Majorana mass eigenstates and the heavy sterile Majorana eigenstates, which can decay into the light ones. The dominant decay mode, into three light neutrinos, is "invisible" because the daughter neutrinos are beyond the detection capabilities of today’s experiments. The most prominent "visible" mode is decay into one active neutrino and one photon, $\nu_s \rightarrow \nu_a \gamma$. Assuming two-neutrino

mixing for simplicity, one can express the inverse width of such a decay as

$$\tau \equiv \Gamma_{\nu_s \rightarrow \nu_a \gamma}^{-1} = 1.3 \times 10^{26} \text{s} \left(\frac{7 \text{ keV}}{m_s} \right)^5 \left(\frac{0.8 \times 10^{-9}}{\sin^2 \theta} \right), \quad (1)$$

where m_s is the mass and θ is the mixing angle. For mass units we set $c = 1$.

Since this is a two-body decay, the photon energy is half the mass of the sterile neutrino. The monochromatic line from dark matter decays can, in principle, be observed by x-ray telescopes. No such observation has been reported, and some important limits have been derived on the allowed masses and mixing angles (Abazajian, Fuller & Patel 2001; Abazajian, Fuller & Tucker 2001; Boyarsky et al. 2005, 2006a,b,c; Riemer-Sørensen et al. 2006; Abazajian 2006b; Watson et al. 2006). These constraints are based on different astrophysical objects, from Virgo and Coma clusters, to Large Magellanic Clouds, to the Milky Way halo and its components, etc. There are different uncertainties in modeling the dark matter populations in these objects. Different groups have also used very different methodologies in deriving these bounds: from a conservative assumption that the dark-matter line should not exceed the signal, to more ambitious approaches that involved modeling the signal or merely fitting it with a smooth curve and requiring that the line-shaped addition not affect the quality of the fit. The x-ray limits are usually shown based on the assumption that the sterile neutrinos constitute the entire dark matter ($\Omega_s = \Omega_{dm}$, where s and dm refer to the sterile neutrinos and the dark matter, respectively). However, the x-ray observations exclude certain masses and mixing angles even if the sterile neutrinos make up only a fraction of dark matter. The production via mixing (Dodelson & Widrow 1994) provides the lowest possible abundance of sterile neutrinos. In Fig. 1 we show both the bounds based on the assumption $\Omega_s = \Omega_{dm}$ and the model-independent exclusion region (Kusenko 2006) based on the production only via the Dodelson & Widrow (1994) mechanism. Kusenko (2006) used the analytical fit to the numerical calculation of Abazajian (2006a), and re-scaled the x-ray flux in proportion to the amount of relic neutrinos produced for a given mass and mixing angle.

A different set of bounds comes from the observations of the Lyman-alpha forest (Viel et al. 2005, 2006; Seljak et al. 2005), which limit the sterile neutrino mass from below. Based on the high-redshift data from SDSS and some modeling of gas dynamics, one can set a limit as strong as 14 keV (Seljak et al. 2005). However, the high-redshift data have systematic errors that are not well understood (Jena et al. 2005), and more conservative approaches, based on the relatively low-redshift data, have led to some less stringent bounds (Viel et al. 2005). More recently, Viel et al. (2006) have reanalyzed the high-redshift data and arrived at the bound $m_s > 10$ keV. The mass bound as quoted depends on the production mechanism in the early universe.

The Lyman-alpha observations constrain the free-streaming lengths of dark matter par-

ticles, not their masses. For each cosmological production mechanism, the relation between the free-streaming length and the mass is different (Hansen et al. 2002). For example, the bound $m_s > 10$ keV (Viel et al. 2006) applies to the production model due to Dodelson & Widrow (1994). Even within a given cosmological scenario, there are uncertainties in the production rates of neutrinos for any given mass and mixing angle (Asaka, Laine & Shaposhnikov 2006). These uncertainties may further affect the interpretation of the Lyman-alpha bounds in terms of the sterile neutrino mass. The x-ray bounds depend on a combination of mass and mixing angle as in eq. (1), regardless of one’s cosmological assumptions, as long as all the dark matter is comprised of sterile neutrinos. However, the x-ray bounds are subject to uncertainties in modeling the dark matter populations of different objects.

If the sterile neutrinos make up only a part of dark matter, none of the above bounds apply. Also, if inflation ended with a low reheating temperature, the bounds are significantly weaker (Gelmini, Palomares-Ruiz & Pascoli 2004).

It should also be mentioned that the Lyman-alpha bounds appear to contradict the observations of dwarf spheroidal galaxies (Wilkinson et al. 2006; Gilmore 2006; Strigari et al. 2006), which suggest that dark matter is warm and which would favor the 1–5 keV mass range for sterile neutrinos. There are several inconsistencies between the predictions of N-body simulations of cold dark matter (CDM) and the observations (Willman et al. 2004; Bode, Ostriker & Turok 2001; Peebles 2001; Dalcanton & Hogan 2001; Bosch & Swaters 2001; Zentner & Bullock 2003; Abazajian, Koushiappas & Zentner 2006; Sommer-Larsen & Dolgov 2001; Governato et al. 2004; Kormendy & Fisher 2005; Fellhauer et al. 2006; Belokurov et al. 2006; Allgood et al. 2006). Each of these problems may find a separate independent solution. Perhaps, a better understanding of CDM on small scales will resolve these discrepancies. It is true, however, that warm dark matter in the form of sterile neutrinos is free from all these small-scale problems altogether, while on large scales WDM fits the data as well as CDM.

Several independent considerations, from the pulsar kicks to small-scale behavior of dark matter, favor sterile neutrinos as the dark matter candidate. It is important, therefore, to examine the effects of sterile-neutrino dark matter on star formation and reionization of the universe. Yoshida et al. (2003) have attempted to study such effects for some kind of warm dark matter, but they have used a linear matter power spectrum and assumed that the dark matter particles have a thermal distribution, which is not the case for sterile neutrinos (Abazajian 2006a). Even more importantly, they have not considered the effects of sterile neutrino decays and the resulting x-ray background. It was shown by Biermann & Kusenko (2006) that the x-rays produced by the decays of relic sterile neutrinos can speed up the formation of molecular hydrogen, which can help the cooling of the gas and the star formation, which can lead, in turn, to a reionization of the universe at the redshift consistent

with the WMAP results.

More specifically, the WMAP (three years) measurement of the reionization redshift $z_r = 10.9_{-2.3}^{+2.7}$ (Spergel et al. 2006) has posed a challenge to theories of star formation. On the one hand, stars have to form early enough to reionize gas at redshift 11. On the other hand, the spectra of bright distant quasars imply that reionization must be completed by redshift 6. Stars form in clouds of hydrogen which collapse at different times, depending on their sizes: the small clouds collapse first, while the large ones collapse last. If the big clouds must collapse by redshift 6, then the small halos must undergo the collapse much earlier. It appears that the star formation in these small halos would have occurred at high redshift, when the gas density was very high, and it would have resulted in an excessive Thompson optical depth (Haiman & Bryan 2006). To be consistent with WMAP, the efficiency for the production of ionizing photons in minihalos must have been at least an order of magnitude lower than expected (Haiman & Bryan 2006). One solution is to suppress the star formation rate in small halos by some dynamical feedback mechanism. The suppression required is by at least an order of magnitude.

Alternatively, one can consider warm dark matter, in which case the number of small clouds is strongly suppressed. However, for some WDM candidates (for example, the gravitino), the lack of power on small scales in the spectrum of density perturbations leads to an unacceptable delay in the onset of star formation (Yoshida et al. 2003). This is not the case for sterile neutrinos, which decay slowly during the "dark ages" preceding the birth of stars. The decay photons could ionize gas, and, although this ionization is too weak to affect the WMAP measurements directly (Mapelli & Ferrara 2005; Mapelli et al. 2006), the increase in the ionization fraction could cause a rapid production of molecular hydrogen at redshifts as high as 100 (Biermann & Kusenko 2006). Molecular hydrogen is the essential cooling agent that allows the gas to cool and collapse to form the first stars.

Biermann & Kusenko (2006) have not considered the effects of gas heating associated with the decays, which may, in some cases, thwart the effects of ionization. The increase in the fraction of molecular hydrogen can help cooling the gas, but if the heating from sterile neutrino decays is significant, it can overcome the radiative cooling and stymie the collapse and star formation. In this paper we will examine thermal evolution of gas clouds in detail, taking into account both effects of the sterile neutrino decays, namely the ionization and the heating of gas.

The paper is organized as follows. In Section 2 we will discuss the role of sterile neutrino decays and the production of molecular hydrogen in the cooling of the primordial gas clouds. Next, in Sections 3-6 we will briefly describe the top-hat overdensity simulation. The results are shown in Section 7.

2. H₂ cooling and sterile neutrinos decays

The existence of the first objects is a direct consequence of the growth of the primordial density fluctuations. At the beginning, there are linear density perturbations which expand with the overall Hubble flow. Subsequently, these perturbations can grow and form primordial clouds. Clouds with enough density contrast decouple from this flow and start to collapse. The kinetic energy of the infalling gas is dissipated through shocks and the cloud becomes pressure supported. The subsequent evolution of the cloud is determined by its ability to cool sufficiently fast. Clouds that do not cool fast enough stay in a pressure-supported state and do not form stars. The existence of the efficient cooling mechanism is necessary to continue the collapse of the cloud, its subsequent fragmentation and star formation.

In the absence of metals, the most important cooling mechanism is cooling by hydrogen atoms and molecules. This mechanism involves the collisional excitation of H or H₂, subsequent spontaneous de-excitation, and photon emission. The emitted photons can escape and take away energy, hence reducing the kinetic energy of the collapsing cloud. Cooling by H dominates for temperatures above 10⁴ K, while the H₂ cooling is more important at lower temperatures. The temperature of the primordial cloud can be higher than 10⁴ K only during a short period of virialization of the baryonic gas. Therefore, H₂ cooling is the most important cooling mechanism during almost entire evolution of the halos, and it is crucial for the star formation.

In primordial gas clouds, H₂ molecules can form mainly through the coupled reactions



or



in which e^- and H^+ act only as a catalyst. X-ray radiation can increase the production of the H₂ by enhancement of the ionization fraction.

As discussed above, sterile neutrinos with the mass of several keV and a small mixing are stable on cosmological time scales. Nevertheless some of them can decay. The decay channel important for us is

$$\nu_s \rightarrow \nu_a + \gamma. \quad (6)$$

Its inverse width is given in equation (1). The energy of the photon is equal to

$$E_0 = \frac{(m_s^2 + m_a^2)}{2m_s} \approx \frac{m_s}{2}, \quad (7)$$

where m_a is the mass of the active neutrino. X-ray photons from the sterile neutrinos decays can increase the ionization fraction and the H_2 production. This can subsequently lead to a speed-up of the gas cooling and star formation.

3. Density evolution

We will follow the evolution of the baryonic top-hat overdensity, the gas temperature and its H_2 and e^- fraction. Our goal is to juxtapose the evolution of the gas temperature in the primordial clouds in the ΛCDM model and the WDM model with keV sterile neutrinos. We assume that the dark matter is smoothly distributed in the region we are considering.

We will use the parameters from the best fit to the three years WMAP data (Spergel et al. 2006), namely $H_0 = 100h \text{ km s}^{-1} \text{ Mpc}^{-3}$, $h = 0.73$, $\Omega_0 = \Omega_{dm} + \Omega_b = 0.238$, $\Omega_b = 0.042$, $\Omega_{dm} = \Omega_0 - \Omega_b = 0.196$, $\Omega_\Lambda = 0.762$, $\Omega_{tot} = \Omega_{dm} + \Omega_b + \Omega_\Lambda = 1$.

Let us take some spherical region with the top-hat overdensity δ . It is well known that such an overdensity will evolve according to the following equation (Padmanabhan 1993)

$$1 + \delta = \frac{9 (\alpha - \sin \alpha)^2}{2 (1 - \cos \alpha)^3}, \quad (8)$$

where the parameter α is related to the redshift z and redshift of virialization z_{vir} through

$$\frac{1 + z_{vir}}{1 + z} = \left(\frac{\alpha - \sin \alpha}{2\pi} \right)^{2/3}. \quad (9)$$

Further evolution depends on the type of the matter in the overdense region. If it is the dark matter then after virialization its density remains constant forever. The situation is different in the case of baryons. If there exists an efficient cooling mechanism, then the density gradually increases. Otherwise, the density remains constant, and there is no star formation in the halo.

In reality an overdense region consists of two components namely, baryonic gas and dark matter. Baryonic density fluctuations are suppressed before recombination. In contrast, the dark matter density fluctuations can start to grow well before this period, so its initial overdensity is larger than that of the baryons. Dark matter forms the potential wells into which the baryonic matter falls. Overall, the baryon density follows the dark matter density in the early universe. Therefore, one can consider the primordial fluctuations as the halos consisting of baryonic and dark matter, whose overall overdensity follow the top-hat solution (eqs. 8 and 9). Of course, this assumption breaks down at the later stages of the halo evolution, e.g. after the virialization of the dark matter.

Following Tegmark et al. (1997), let us assume that the evolution of the baryonic and dark matter density is described by equations (8) and (9) until α reaches $3\pi/2$. This occurs at the redshift

$$z_{3\pi/2} = 1.06555 (1 + z_{vir}) - 1. \quad (10)$$

After this redshift, we assume that the density of the halo ρ_{b+dm} stays constant e.g. it is equal to the value

$$\rho_{b+dm} = 18\pi^2 \Omega_0 \rho_0 (1 + z_{vir})^3, \quad (11)$$

where ρ_0 is the critical density of the universe.

We note that the overdensity δ in equation (8) is given by

$$\delta = \frac{\rho_{b+dm}}{\bar{\rho}} - 1, \quad (12)$$

where $\bar{\rho}$ is the combined average density of dark and baryonic matter.

We have taken the ratio of the baryonic to the dark matter mass in the halo to be the standard cosmological ratio of $\Omega_b/\Omega_{dm} \approx 0.214$. The density of the baryonic matter can be expressed as

$$\rho_b = \rho_{b+dm} \frac{\Omega_b}{\Omega_0}. \quad (13)$$

4. Temperature evolution

The gas temperature evolution is governed by the equation of energy conservation

$$\frac{du}{dt} = \frac{p}{\rho_b^2} \frac{d\rho_b}{dt} - \frac{\Lambda}{\rho_b}, \quad (14)$$

where p , u and Λ are the pressure, the internal energy per unit mass and the cooling/heating function respectively. We use the equation of state of perfect gas

$$p = (\gamma - 1) \rho_b u, \quad (15)$$

where γ is the adiabatic index.

The internal energy per unit mass can be described as

$$u = \frac{1}{\gamma - 1} \frac{kT}{\mu m_H}, \quad (16)$$

where k is the Boltzmann constant, T is the gas temperature, μ denotes the molecular weight, and m_H is the mass of the hydrogen atom. Introducing the number density of non dark matter particles n_p we can write ρ_b as

$$\rho_b = \mu m_H n_p. \quad (17)$$

If we use eqs. (15), (16) and (17) than we can cast eq. (14) in the form

$$\frac{dT}{dt} = (\gamma - 1) \left(\frac{T}{n_p} \frac{dn_p}{dt} - \frac{\Lambda}{n_p k} \right) + \gamma \frac{T}{\mu} \frac{d\mu}{dt} + \frac{T}{(\gamma - 1)} \frac{d\gamma}{dt}. \quad (18)$$

The time t can be translated to the redshift z in the following way

$$\frac{dt}{dz} = - \frac{1}{H_0 (1+z) \sqrt{\Omega_\Lambda + \Omega_0 (1+z)^3}}. \quad (19)$$

Using eqs. (18) and (19), we obtain

$$\frac{dT}{dz} = (\gamma - 1) \frac{T}{n_p} \frac{dn_p}{dz} + \gamma \frac{T}{\mu} \frac{d\mu}{dz} + \frac{T}{(\gamma - 1)} \frac{d\gamma}{dz} + \frac{(\gamma - 1) \Lambda}{n_p k H_0 (1+z) \sqrt{\Omega_\Lambda + \Omega_0 (1+z)^3}}. \quad (20)$$

To calculate the gas temperature of the primordial cloud we have to integrate this equation.

One can assume that the gas temperature evolution is governed by eq. (20) except for the redshift range between $z_{3\pi/2}$ and z_{vir} . If we simply integrate eq.(20) to the redshift z_{vir} , than the gas temperature will be much lower than the virial temperature T_{vir} , at least for clouds with mass greater than some critical value (Kitayama et al. 2001)

$$T_{vir} = 9.09 \times 10^3 \text{ K} \left(\frac{\mu_{vir}}{0.59} \right) \left(\frac{M_{b+dm}}{10^9 h^{-1} M_\odot} \right)^{2/3} \left(\frac{\Delta_c(z_{vir})}{18\pi^2} \right)^{1/3} (1 + z_{vir}), \quad (21)$$

where μ_{vir} , M_{b+dm} and $\Delta_c(z_{vir})$ are respectively the mean molecular weight during virialization, the halo mass and the overdensity of the halo at virialization given by (Bryan & Norman 1998), which is very well approximated by $18\pi^2$ for redshifts $z_{vir} \leq 100$. Therefore we have to take into account shocks and increase the gas temperature to the virial value. It is reasonable to assume that the gas temperature evolution is linear between the redshift $z_{3\pi/2}$ and z_{vir} and is described by the equation

$$\frac{dT}{dz} = \frac{T_{vir} - T_{3\pi/2}}{z_{vir} - z_{3\pi/2}}, \quad (22)$$

where $T_{3\pi/2}$ is the temperature at the redshift $z_{3\pi/2}$.

Let us consider the following five species: H, H⁺, H₂, e⁻, and He with the mass fraction $Y = 0.244$ (Izotov & Thuan 1998). Let us denote by n_i ($i = \text{H, H}^+, \text{H}_2, e^-, \text{He}$) the number density of baryonic component i . We assume that $n_{\text{H}^+} = n_e$ e.g. there is no He or H₂ ionization. The number density of hydrogen can be written as

$$n = n_H + n_{\text{H}^+} + 2n_{\text{H}_2}. \quad (23)$$

If we introduce the number fraction of component "i"

$$x_i = \frac{n_i}{n}, \quad (24)$$

then the particle number density n_p and the baryon density ρ_b are equal to

$$n_p = n \left(1 + \frac{Y}{4X} - x_{\text{H}_2} + x_e \right) \quad (25)$$

and

$$\rho_b = \frac{nm_H}{X}, \quad (26)$$

where $X = 1 - Y = 0.756$ is the hydrogen mass fraction.

Using eqs. (17), (25) and (26) we can get

$$\mu = \frac{1}{X(1 + x_e - x_{\text{H}_2}) + 0.25Y}. \quad (27)$$

At the virialization we have typically $x_{\text{H}_2} \approx 0$ and $x_e \approx 1$, so one can take the mean molecular weight at this time to be $\mu_{\text{vir}} = 1/(2X + 0.25Y) \approx 0.63$. We can express γ as

$$\gamma = 1 + \left(\sum_{i=1}^5 n_i \right) / \left(\sum_{i=1}^5 \frac{n_i}{\gamma_i - 1} \right), \quad (28)$$

where $\gamma_H = \gamma_{\text{H}^+} = \gamma_e = \gamma_{\text{He}} = 5/3$ and $\gamma_{\text{H}_2} = 7/5$.

5. Chemical reactions and cooling/heating function

To calculate the cooling/heating function Λ in eq. (20) we have to take into account all of the relevant chemical and thermal processes and follow the number density evolution of different baryonic components. All chemical and thermal processes included in our calculation are summarized in Tables 1 and 2. The evolution of x_e and x_{H^+} is described by equations

$$\frac{dx_e}{dt} = (A(z) + k_{12} + k_{14}n_e) x_H - k_{13}x_e^2n \quad (29)$$

$$\frac{dx_{H^+}}{dt} = \frac{dx_e}{dt}, \quad (30)$$

where $A(z)$ is the production rate of free electrons by the sterile neutrino decays which is calculated in the appendix. In eq. (29) Only the ionization and recombination of hydrogen are included. All the rates k_i are given in Table 1.

We note in passing that neglecting He and H_2 ionization renders the system with fewer free electrons, so the production of H_2 is slower. In addition, cooling by H_2^+ is stronger than by H_2 (see last figure in Galli & Palla (1998)). Therefore, the cooling we get in this approximation is somewhat less efficient than it should be in reality.

The molecular hydrogen number fraction can be calculated by integration of the following equation

$$\frac{dx_{H_2}}{dt} = n_H (x_e k_m - k_7 x_{H_2}) - (k_8 x_{H_2} + k_9 x_e) n_{H_2} - (k_{10} + k_{11}) x_{H_2}, \quad (31)$$

where

$$k_m = \frac{k_1 k_2}{k_2 + k_3/n_H} + \frac{k_4 k_5}{k_5 + k_6/n_H} \quad (32)$$

is the molecular hydrogen formation rate via H^- and H_2^+ channel (Tegmark et al. 1997). To get eq. (32) we have to make the assumption that after formation of H^- and H_2^+ they are used almost instantaneously in the next reactions (reactions number 2 and 3 or 5 and 6 respectively, see Table 1). This is a very good approximation, because in reality the H^- and H_2^+ fractions always remain small.

The cooling/heating function Λ is given in the appendix (eq. C3). It includes contributions from the following processes:

1. excitation of H by collisions with e^-
2. recombination to H
3. ionization of H by collisions with e^-
4. photo-ionization of H by the CMB radiation
5. excitation of H_2 by collisions with H and H_2
6. H_2 formation cooling
7. dissociation of H_2 by collisions with H, H_2 and e^-
8. photo-dissociation of H_2 by CMB photons

9. Compton cooling
10. bremsstrahlung
11. photo-ionization of H by the photons from the sterile neutrino decays and H ionization by the secondary electrons produced due to these photons

We have not included the effect of the photo-dissociation of H_2 by the photons from the sterile neutrino decays. This is because the flux of these photons is small in comparison with the CMB radiation in the 10 - 30 eV range, which is the energy range relevant to the photo-dissociation of H_2 .

The formulae for the contributions to the Λ function from all of these processes are given in Table 2. We have assumed the ortho- H_2 to para- H_2 ratio to be 3 : 1.

6. Initial conditions and numerical procedure

We start our calculations at the redshift of recombination $z_{rec} = 1013$, taking as initial conditions $x_e = 1$, $x_{H_2} = 0$ and assuming that the gas temperature is equal to the CMB temperature. Evolution of the halo is insensitive for the initial value of x_{H_2} .

We follow the evolution of the density, eqs. (8) and (9), and the temperature, eq. (20) with the cooling/heating function given in eq. (C3) until the redshift is equal to $z_{3\pi/2}$, *cf.* eq. (10). From that time we assume that the density of the halo stays constant and is equal to its virial value (11). We assume that the gas starts to be shock heated in this period and reaches its virial temperature at z_{vir} . The temperature of the gas is assumed to change linearly with the redshift between $z_{3\pi/2}$ and z_{vir} , eq. (22). For the redshift lower than z_{vir} the gas temperature is calculated once again by integration of eq. (20).

Following Tegmark et al. (1997), we use the following criterion for the successful collapse:

$$T(\eta z_{vir}) \leq \eta T(z_{vir}), \quad (33)$$

where $\eta = 0.75$ (Tegmark et al. 1997).

7. Results

The results of our analysis depend, of course, on the parameters we choose for the dark-matter sterile neutrinos. The x-ray flux, and the resulting increase in the ionization

fraction depend on the combination ($m_s^5 \sin^2 \theta$). The power spectrum on small scales, which determines the presence or absence of small clouds, depends on the free-streaming length, which is set by the mass (in every given cosmological scenario).

Based in part on the existing limits, we have chosen four illustrative benchmark cases to illustrate the effects of ionization and heating due to sterile neutrino decays on the cloud collapse.

We have compared the following four models:

1. Cold dark matter with no additional radiation besides CMB (CDM).
2. Warm dark matter (WDM) with the sterile neutrino mass $m_s = 25$ keV and mixing angle $\sin^2 \theta = 3 \times 10^{-12}$ (WDM1).
3. WDM with $m_s = 15$ keV and $\sin^2 \theta = 3 \times 10^{-12}$ (WDM2).
4. WDM with $m_s = 3.3$ keV and $\sin^2 \theta = 3 \times 10^{-9}$ (WDM3).

The values of parameters chosen for these models are shown in Fig.1.

Some comments are in order. The choice of WDM1 is obvious because it satisfies all the constraints, including the x-ray bounds and the Lyman-alpha bounds. The masses as large as $m_s = 25$ keV cannot be constrained by either Chandra or XMM, and the best constraint comes from HEAO, which is weaker because of its lower energy resolution (Boyarsky et al. 2005, 2006a,b,c). Also, WDM1 corresponds to a very small free-streaming length and, on large scales, it creates structure indistinguishable from CDM. The only difference between WDM1 and CDM is the additional x-ray flux. Therefore, the comparison of CDM and WDM1 cases provides a clean test of the effects of the increased ionization fraction (Biermann & Kusenko 2006). Also, WDM1 provides a realistic set of parameters consistent with all the bounds, as well as the pulsar kick mechanism due to resonant active-sterile neutrino conversions (Kusenko & Segrè 1997).

WDM2 is also consistent with all the existing limits, including the most ambitious Lyman-alpha bounds (Seljak et al. 2005). (We remind the reader that Viel et al. (2006) have obtained a 50% weaker limit using the same data.) The x-ray background is lower in this case than in the case of WDM1.

Finally, WDM3 corresponds to masses that would be ruled out by the "strong" Lyman-alpha bounds obtained by Seljak et al. (2005) and by Viel et al. (2006). However, one has to remember that the relation between the masses and the free-streaming length depends

on the production mechanism of sterile neutrinos. For example, the free-streaming length in the Shi & Fuller (1999) production mechanism is different from the Dodelson & Widrow (1994) mechanism. Even within the latter framework, additional entropy production can redshift the sterile neutrino momenta and eliminate the Lyman-alpha bound (Asaka, Kusenko & Shaposhnikov 2006). If dark matter is produced from a coupling between the sterile neutrinos and the inflaton (Shaposhnikov & Tkachev 2006), the free-streaming length is, again, different. WDM3 requires redshifting of the neutrino momenta by a factor ~ 3 , as compared to the thermal distribution. This can be achieved, for example, by entropy production of the order of 10^2 , which is comparable to the effect of change in the number of degrees of freedom from the electroweak scale to zero temperature (Kusenko 2006). Hence, WDM3 should not be considered an unrealistic scenario. In addition, WDM3 is of interest because it is consistent with the pulsar kick mechanism via off-resonant active-sterile neutrino oscillations (Fuller et al. 2003), even if this sterile neutrino is not the dominant component of dark matter.

The results of the calculation are presented in Figures 2, 3 and 4. Several conclusions can be drawn from these results. We find that large clouds, with masses greater than $10^{10}M_\odot$, collapse regardless of the details of cooling in all the models defined above. One could expect this behavior because the virial temperature of such a cloud is higher than 10^4 K, so the H cooling mechanism is efficient enough and the additional H_2 does not play an important role.

There is, however, a dramatic difference when it comes to smaller clouds. For a virialization redshift $z_{vir} = 20$, a cloud of $4 \times 10^5 M_\odot$ collapses in model WDM1, but not in the CDM or other WDM models. This illustrates the importance of the increased H_2 fraction on the cooling of gas.

In WDM2 and WDM3 model, because of the relatively low associated x-ray flux, the temperature evolution is practically unaffected by the photons from the dark matter decay.

From Fig. 4 one can draw another conclusion. In the large clouds, all of the H_2 molecules are destroyed during the virialization process. This is because of the very high virial temperature. In contrast, there is a drastic increase in H_2 fraction during the virialization of the clouds with the mass of $4 \times 10^5 M_\odot$. In both cases, most of molecular hydrogen is produced after virialization.

For clouds with $M = 4 \times 10^5 M_\odot$ and $z_{vir} = 100$ the critical H_2 fraction (see eq. (11) of Tegmark et al. 1997) is reached at virialization. On the other hand, in the clouds having equivalent mass with $z_{vir} = 20$, the molecular hydrogen fraction x_{H_2} attains its virial critical value only for WDM1 model. This happens at $z = 7.5$.

In all the WDM models the ionization and the molecular hydrogen fraction are enhanced in comparison with the CDM model, as suggested by Biermann & Kusenko (2006). In addition, we can see that in WDM models the temperature of the collapsing clouds soon after virialization is lower than that in the CDM case, which speeds up the collapse, at least for the low-mass clouds.

We note in passing that the density of the cloud was kept constant after virialization, so the evolution of T , x_e and x_{H_2} is reliable for the redshifts close to virialization, but not for much smaller redshifts.

It appears that WDM3 model is disfavored. The increase in the cooling rate is almost negligible in comparison with the CDM case, while the suppression on the small scales is very strong. Therefore, this leads to an unacceptable delay in the onset of star formation, as discussed by Yoshida et al. (2003).

In the case of WDM1 and WDM2 models, the cooling is enhanced by the additional fraction of molecular hydrogen. However, we cannot definitively prove that star formation occurs at the redshift consistent with WMAP because of the simplifying assumptions and limitations of our analysis.

The main limitation is that the virialization redshift of a particular cloud is a fixed parameter in the simulation. In reality, it can be changed by the enhancement of the cooling, so the cloud can reach its virial stage much earlier. Moreover, the density of the cloud is kept constant after virialization, which is a simplifying assumption. We can not calculate the real redshift of the cloud collapse and onset of the star formation. As a result, we cannot calculate how many clouds collapse at a given redshift and we cannot calculate the redshift of reionization in WDM model reliably. Also, we have not included the additional x-rays from the decay of sterile neutrinos inside the collapsing clump. This radiation can cause an additional increase in ionization and heating, which could change our results. Also the effects of opacity can be important in large clouds, which we have not taken into account. These limitations will be addressed in the future work.

8. Conclusions

We have performed a detailed analysis of the cooling and collapse of primordial gas in the model with warm dark matter, taking into account both the increase in the fraction of molecular hydrogen (Biermann & Kusenko 2006) and the heating due to the sterile neutrino decay. As expected, the effect on the largest gas clouds is negligible, but the smaller clouds are, in fact affected. We have performed the analysis for some benchmark cases which arise

in realistic scenarios. For the largest clouds, the additional molecular hydrogen made no difference. For smaller clouds, especially for those with masses $10^5 - 10^6 M_\odot$, the increase in the x-ray background made the successful collapse possible in cases where it could not occur in the absence of sterile neutrino decays.

Acknowledgments

We thank G. Gilmore, M. Mapelli, M. Shaposhnikov, and S. Stachniewicz for very helpful discussions and comments. The work of P.L.B. and J.S. was supported by the Pierre Auger grant 05 CU 5PD1/2 via DESY/BMBF. The work of A.K. was supported in part by the DOE grant DE-FG03-91ER40662 and by the NASA ATP grants NAG 5-10842 and NAG 5-13399. A.K. thanks the CERN Theory unit and EPFL for hospitality during his visit. J.S. thanks the organizers of Marcel Grossmann meeting for support.

Appendix

A. Specific intensity of the photons from the sterile neutrino decays

In this section we shall calculate the photon spectrum produced by the radiative decays of the sterile neutrinos (our derivation is similar to the one in Masso & Toldra (1999)). The dominant channel of radiative decays is through the following reaction

$$\nu_s \rightarrow \nu_a + \gamma, \tag{A1}$$

where ν_s is the sterile neutrino and ν_a is an ordinary active neutrino. The photon energy is given by

$$E_0 = \frac{(m_s^2 + m_a^2)}{2m_s} \approx \frac{m_s}{2}, \tag{A2}$$

where m_s and m_a are respectively the mass of the sterile and an active neutrino. The cosmic expansion redshifts the photon energy. A photon that at redshift z has energy E was produced at redshift z_0 given by

$$1 + z_0 = (1 + z) \frac{E_0}{E}. \tag{A3}$$

Let $F_E(z)$ be the energy flux (in units of $\text{erg cm}^{-2} \text{s}^{-1}$) at redshift z of photons with energy E produced by the sterile neutrino decays. The flux per unit energy and solid angle is given by

$$\frac{d^2 F_E(z)}{dE d\Omega} = E \frac{d^2 F_n(z)}{dE d\Omega}, \tag{A4}$$

where $F_n(z)$ is the photon flux at redshift z . It is related to the photon flux at emission redshift z_0 through the following equation

$$\frac{d^2 F_n(z)}{d\Omega} = \left(\frac{1+z}{1+z_0}\right)^3 \frac{d^2 F_n(z_0)}{d\Omega} = \frac{1}{4\pi} \left(\frac{1+z}{1+z_0}\right)^3 \delta n_\gamma(z_0) c, \quad (\text{A5})$$

where we have included the factor of $\left(\frac{1+z}{1+z_0}\right)^3$ produced by the expansion of the universe. The photon density emitted at z_0 is given by the usual decay law

$$\delta n_\gamma(z_0) = \frac{\delta t}{\tau} \tilde{n}_s(z_0), \quad (\text{A6})$$

where τ is the mean sterile neutrino lifetime for the decay into an active neutrino and a photon (see eq. 1), $\tilde{n}_s(z_0)$ is the number density of the sterile neutrino at redshift z_0 and δt is given by

$$\delta t = \frac{dt}{dz_0} dz_0 = -\frac{dz_0}{H_0(1+z_0)\sqrt{\Omega_\Lambda + \Omega_0(1+z_0)^3}} = \frac{1}{H(z_0)} \frac{dE}{E}, \quad (\text{A7})$$

where $H(z_0) = H_0\sqrt{\Omega_\Lambda + \Omega_0(1+z_0)^3}$ is the Hubble expansion rate at photon emission redshift z_0 . Writing everything together we obtain

$$\frac{d^2 F_E(z)}{dE d\Omega} = \frac{1}{4\pi} \left(\frac{1+z}{1+z_0}\right)^3 \frac{\tilde{n}_s(z_0) c}{\tau H(z_0)}. \quad (\text{A8})$$

Choosing the time $t_p \ll \tau$ otherwise arbitrary we can write

$$\left(\frac{1+z}{1+z_0}\right)^3 \tilde{n}_s(z_0) = \left(\frac{1+z}{1+z_p}\right)^3 \tilde{n}_s(z_p) \exp\left(\frac{t_p - t(z_0)}{\tau}\right) = n_s(z) \exp\left(\frac{t_p - t(z_0)}{\tau}\right) \quad (\text{A9})$$

where $t(z_0)$ is the age of the universe at redshift z_0 , $t_p = t(z_p)$ and $n_s(z)$ would be the number density of sterile neutrinos at redshift z if they did not decay.

Assuming that all of the dark matter consists of sterile neutrinos, $n_s(z)$ can be written as

$$n_s(z) = n_s^0 (1+z)^3, \quad (\text{A10})$$

where

$$n_s^0 = \Omega_{dm} \frac{\rho_0}{m_s}. \quad (\text{A11})$$

In the case of a flat universe filled with matter and a nonvanishing cosmological constant the age of the universe at redshift z is given by (Masso & Toldra 1999)

$$t(z) = \frac{2}{3H_0\sqrt{\Omega_\Lambda}} \ln \frac{\sqrt{\Omega_\Lambda} + \sqrt{\Omega_\Lambda + \Omega_0(1+z)^3}}{\sqrt{\Omega_0(1+z)^3}}. \quad (\text{A12})$$

Taking $t_p = 0$ and substituting eq. (A9) into eq. (A8) we can get the specific intensity (in units of $\text{erg cm}^{-2} \text{s}^{-1} \text{sr}^{-1} \text{Hz}^{-1}$) of the photons with frequency ν from the sterile neutrino decays at redshift z

$$I_\nu(z) = h \frac{d^2 F_E(z)}{dE d\Omega} = \frac{h n_s(z) c}{4\pi \tau H(z_0)} \exp\left(\frac{-t(z_0)}{\tau}\right). \quad (\text{A13})$$

We have to multiply this value by $e^{-\tau_{abs}(z, z_0)}$ in order to correct specific intensity for the absorption by the background neutral hydrogen atoms. The optical depth is given by

$$\tau_{abs}(z, z_0) = \int_z^{z_0} \sigma_{12}(E(z')) n_H(z') c \frac{dt}{dz'} dz', \quad (\text{A14})$$

where $\sigma_{12}(E(z'))$ and $n_H(z')$ are the cross section for the H ionization at energy $E(z')$ and the hydrogen number density of the Universe at redshift z' respectively; $E(z')$ is the energy of the photon at redshift z' , which was emitted in sterile neutrino decay at redshift z_0 and is given by the equation

$$E(z') = \frac{1+z'}{1+z_0} E_0. \quad (\text{A15})$$

The mean hydrogen number density of the Universe at redshift z' can be written as

$$n_H(z') = n_H^0 [1 - x_e(z)] (1+z')^3, \quad (\text{A16})$$

where n_H^0 is its present value and is equal to

$$n_H^0 = \frac{\Omega_b \rho_0 X}{m_H}. \quad (\text{A17})$$

The cross section for the H ionization is given by

$$\sigma_{12}(E(z')) = \sigma_0 \left(\frac{h\nu_{th}^H}{E(z')} \right)^3, \quad (\text{A18})$$

where $\sigma_0 = 7.909 \times 10^{-18} \text{ cm}^{-2}$ and $h\nu_{th}^H = 13.6 \text{ eV}$.

Neglecting the Ω_Λ term in eq. (19), which is a very good approximation at high redshifts, and using eqs. (A3), (A15), (A16) and (A18) we can cast eq. (A14) into the form

$$\tau_{abs}(z, z_0) = \sigma_0 \left(\frac{h\nu_{th}^H}{E} \right)^3 (1+z)^3 n_H^0 c H_0^{-1} \Omega_0^{-1/2} \int_z^{z_0} [1 - x_e(z')] (1+z')^{-5/2} dz'. \quad (\text{A19})$$

As $x_e(z)$, let us take

$$x_e(z) = \begin{cases} 0 & z < z_{rec} \\ 1 & z > z_{rec} \end{cases}, \quad (\text{A20})$$

where z_{rec} is the recombination redshift. It gives us

$$\tau_{abs}(z, z_0) = \frac{2}{3}\sigma_0 \left(\frac{\nu_{th}}{\nu}\right)^3 (1+z)^{3/2} n_H^0 c H_0^{-1} \Omega_0^{-1/2} \left[1 - \left(\frac{1+z}{1+\min(z_0, z_{rec})}\right)^{3/2}\right]. \quad (\text{A21})$$

Photons emitted before recombination are Compton scattered and thermalized. For simplicity we assume that these photons are not visible. The final specific intensity is equal to

$$I_\nu(z) = \begin{cases} \frac{hcn_s(z)e^{-\frac{t(z_0)}{\tau}}e^{-\tau_{abs}(z, z_0)}}{4\pi\tau H_0\sqrt{\Omega_\Lambda+\Omega_0(1+z)^3}\left(\frac{E_0}{h\nu}\right)^3} & h\nu > E_0\frac{1+z}{1+z_{rec}} \\ 0 & h\nu < E_0\frac{1+z}{1+z_{rec}} \end{cases}, \quad (\text{A22})$$

where

$$t(z_0) = t\left(\frac{E_0}{h\nu}(1+z) - 1\right), \quad (\text{A23})$$

$$\tau_{abs}(z, z_0) = \tau_{abs}\left(z, \frac{E_0}{h\nu}(1+z) - 1\right). \quad (\text{A24})$$

We have assumed that the photons are absorbed only by the Ly α wedge, so the above equations are valid only for $h\nu > 13.6$ eV. To derive the photon flux at energy lower than 13.6 eV we have to take into account another hydrogen absorption lines. The radiation with energy below 13.6 eV start to be important only at lower redshifts (e.g. for $m_s = 5$ keV at $z \approx 5$) so it is not relevant in our calculations.

B. Heating and ionization due to the sterile neutrino decays

The photons from the decays of the sterile neutrino are mainly absorbed by neutral hydrogen atoms leading to their ionization. The ionization rate due to these photons is enhance almost 100 times due to additional ionization by the secondary electrons which deposit almost 1/3 of its energy into ionization (depending on the ionization fraction of the medium). The energy of the absorbed photons partially goes into ionization and partially into heating and excitations. We have adopted the approximation by Shull & Steenberg (1985), for which ionization rate and heating due to the photons from the decays of the sterile neutrino are respectively equal to

$$A(z) = \left[\int_{\nu_{th}^H}^{\infty} 4\pi\sigma_H(\nu) \frac{I_\nu(z)}{h\nu} \left(\frac{h\nu - h\nu_{th}^H}{h\nu_{th}^H}\right) d\nu + \frac{Y}{4X} \int_{\nu_{th}^{He}}^{\infty} 4\pi\sigma_{He}(\nu) \frac{I_\nu(z)}{h\nu} \left(\frac{h\nu - h\nu_{th}^{He}}{h\nu_{th}^H}\right) d\nu \right]$$

$$\times C_i (1 - x_e^{a_i})_i^b + \int_{\nu_{th}^H}^{\infty} 4\pi\sigma_H(\nu) \frac{I_\nu(z)}{h\nu} d\nu \quad (\text{B1})$$

$$\begin{aligned} \Gamma_s(z) &= \left[\int_{\nu_{th}^H}^{\infty} 4\pi\sigma_H(\nu) \frac{I_\nu(z)}{h\nu} (h\nu - h\nu_{th}^H) d\nu \right. \\ &\quad \left. + \frac{Y}{4X} \int_{\nu_{th}^{He}}^{\infty} 4\pi\sigma_{He}(\nu) \frac{I_\nu(z)}{h\nu} (h\nu - h\nu_{th}^{He}) d\nu \right] \\ &\times C_h \left[1 - (1 - x_e^{a_h})_h^b \right] n_H, \end{aligned} \quad (\text{B2})$$

where

$$\sigma_{He}(\nu) = 7.83 \times 10^{-18} \text{cm}^{-2} \left[1.66 \left(\frac{\nu_{th}^{He}}{\nu} \right)^{2.05} - 0.66 \left(\frac{\nu_{th}^{He}}{\nu} \right)^{3.05} \right] \quad (\text{B3})$$

is the cross section for He ionization, $h\nu_{th}^{He} = 24.6$ eV is its energy threshold; $C_i = 0.3908$, $a_i = 0.4092$, $b_i = 1.7592$, $C_h = 0.9971$, $a_h = 0.2663$, $b_h = 1.3163$ (Shull & Steenberg 1985).

C. Cooling/heating function

The H_2 cooling function (Λ_{H-H_2} , $\Lambda_{H_2-H_2}$ and Λ_{form}) given in Table 2 has been computed assuming that the CMB temperature is much smaller than the gas temperature. This approximation is not valid in our case since in the WDM model with keV sterile neutrinos the gas temperature can be very close or even lower than the CMB temperature because of relatively high ionization fraction. The situation is very similar in CDM model, where the gas temperature strictly follows the CMB temperature at least at high redshifts.

In such conditions, the level population of H_2 is strongly affected by stimulated emission and absorption. Molecules become an effective heating source for the gas, because the rate of collisional de-excitation of the vibrational levels is faster than their radiative decay. In order to correct the cooling/heating function for this effect, we have to take the net cooling rate

$$\Lambda_i(T, T_r) = \Lambda_i(T) - \Lambda_i(T_r), \quad (\text{C1})$$

where Λ_i represents either Λ_{H-H_2} , $\Lambda_{H_2-H_2}$, or Λ_{form} . We also note that $\Lambda_i(T, T_r) \approx \Lambda_i(T)$ for $T \gg T_r$.

One should do the same for the Λ_{H-e} (see Table 2). However, the cooling from the collisional excitation of hydrogen atoms H and its subsequent spontaneous de-excitation is only important for the gas temperatures $T > 10^4$. In our case the CMB temperature is well below 10^4 K, so we can neglect the heating term for this cooling/heating mechanism.

For completeness we have to take also into account the fact that electrons can gain energy from the CMB radiation when $T < T_r$, so we are taking as the bremsstrahlung cooling/heating term

$$\Lambda_{brem}(T, T_r) = \Lambda_{brem}(T) - \Lambda_{brem}(T_r). \quad (\text{C2})$$

In our calculations we have used the following cooling/heating function:

$$\begin{aligned} \Lambda(T, T_r, z) &= \Lambda_H(T, T_r) + \Lambda_{H_2}(T, T_r) + \Lambda_{comp}(T, T_r) \\ &+ \Lambda_{brem}(T, T_r) + \Lambda_s(z). \end{aligned} \quad (\text{C3})$$

REFERENCES

- Abazajian, K. 2006a, Phys. Rev. D, 73, 063506
- Abazajian, K. 2006b, Phys. Rev. D, 73, 063513
- Abazajian, K., Fuller, G. M., & Patel, M. 2001, Phys. Rev. D, 64, 023501
- Abazajian, K., Fuller, G. M., & Tucker, W. H. 2001, ApJ, 562, 593
- Abazajian, K., Koushiappas, S. M., & Zentner, A. R. 2006, private communication
- Abel, T., Anninos, P., Zhang, Yu., & Norman, M. L. 1997, New A, 2, 181
- Akhmedov, E. K., Rubakov, V. A., & Smirnov, A. Y. 1998, Phys. Rev. Lett., 81, 1359
- Allgood, B., Flores, R. A., Primack, J. R., Kravtsov, A. V., Wechsler, R. H., Faltenbacher, A., & Bullock, J. S. 2006, MNRAS, 367, 1781
- Appelquist, T. & Shrock, R. 2002, Phys. Lett. B 548, 204
- Asaka, T., Kusenko, A., & Shaposhnikov, M. 2006, arXiv:hep-ph/0602150
- Asaka, T., Laine, M., & Shaposhnikov, M. 2006, arXiv:hep-ph/0605209
- Asaka, T., Blanchet, S., & Shaposhnikov, M. 2005, Phys. Lett. B, 631, 151
- Asaka, T., & Shaposhnikov, M. 2005, Phys. Lett. B, 620, 17
- Athanassopoulos, C., et al. (LSND) 1998, Phys. Rev. Lett., 81, 1774
- Barkovich, M., D’Olivo, J. C., & Montemayor, R. 2004, Phys. Rev. D, 70, 043005

- Barkovich, M., D’Olivo, J. C., & Montemayor, R. 2005, in *New Research*, Nova Science Publishers [arXiv:hep-ph/0503113]
- Belokurov, V., et al. 2006, ApJ, 642, L137
- Biermann, P. L., & Kusenko, A. 2006, Phys. Rev. Lett., 96, 091301
- Bode, P., Ostriker, J. P., & Turok, N. 2001, ApJ, 556, 93
- van den Bosch, F. C., & Swaters, R. A. 2001, MNRAS, 325, 1017
- Boyarsky, A., Neronov, A., Ruchayskiy, O., & Shaposhnikov, M. 2005, arXiv:astro-ph/0512509
- Boyarsky, A., Neronov, A., Ruchayskiy, O., & Shaposhnikov, M. 2006a, JETP Lett. 83, 133
- Boyarsky, A., Neronov, A., Ruchayskiy, O., & Shaposhnikov, M. 2006b, arXiv:astro-ph/0603368
- Boyarsky, A., Neronov, A., Ruchayskiy, O., Shaposhnikov, M., & Tkachev, I. 2006c, arXiv:astro-ph/0603660
- Bryan, G. L., & Norman, M. L. 1998, ApJ, 495, 80
- Dalcanton, J. J., & Hogan, C. J. 2001, ApJ, 561, 35
- de Gouvêa, A., Phys. Rev. D 72, 033005 (2005).
- Dodelson, S., & Widrow, L. M. 1994, Phys. Rev. Lett., 72, 17
- Dolgov, A. D., & Hansen, S. H. 2002, Astropart. Phys., 16, 339
- Fan, X., et al. 2001, AJ, 122,2833
- Farzan, Y., Peres, O. L. G., & Smirnov, A. Y. 2001, Nuclear Physics B, 612, 59
- Fellhauer, M., et al. 2006, arXiv:astro-ph/0605026
- Fryer, C. L., & Kusenko, A. 2006, ApJS., 163, 335
- Fuller, G. M., Kusenko, A., Mocioiu, I., & Pascoli, S. 2003, Phys. Rev. D, 68, 103002
- Galli, D., & Palla, F. 1998, A&A, 335, 403
- Gell-Mann, M., Ramond, P., & Slansky, R. 1979, in *Supergravity*, ed. by Freedman, D., et al., North Holland

- Gelmini, G., Palomares-Ruiz, S., & Pascoli, S. 2004, *Phys. Rev. Lett.*, 93, 081302
- Gilmore, G., in proceedings of *7th UCLA Symposium On Sources And Detection Of Dark Matter And Dark Energy In The Universe*, 22-24 Feb 2006, Marina de Rey, California, to appear.
- Governato, F., et al. 2004, *ApJ*, 607, 688
- Haiman, Z., Thoul, A. A., & Loeb, A. 1996, *ApJ*, 464, 523
- Haiman, Z., & Bryan, G. L. 2006, arXiv:astro-ph/0603541
- Hansen, S. H., Lesgourgues, J., Pastor, S., & Silk, J. 2002, *MNRAS*, 333, 544
- Hollenbach, D., & McKee, C. F. 1979, *ApJS*, 41, 555
- Izotov, Y. I., & Thuan, T. X. 1998, *ApJ*, 500,188
- Kitayama, T., Susa, H., Umemura, M., & Ikeuchi, S. 2001, *MNRAS*, 326, 1353
- Kormendy, J., & Fisher, D. B. 2005, in *Revista Mexicana de Astronomia y Astrofisica Conference Series*, pp. 101-108, arXiv:astro-ph/0507525
- Kusenko, A., & Segrè, G. 1997, *Phys. Lett. B*396, 197
- Kusenko, A., & Segrè, G. 1999, *Phys. Rev. D*, 59, 061302
- Kusenko, A., Segrè, G., & Vilenkin, A. 1998, *Phys. Lett. B*437, 359
- Kusenko, A. 2004, *IJMP D* 13, 2065
- Kusenko, A. 2006, arXiv:hep-ph/0609081
- Jena, T., et al. 2005, *MNRAS*, 361, 70
- Lenzuni, P., Chernoff, D. F., & Salpeter, E. E. 1991, *ApJS*, 76, 759
- Mapelli, M., & Ferrara, A. 2005, *MNRAS*, 364, 2
- Mapelli, M., Ferrara, A., & Pierpaoli, E. 2006, arXiv:astro-ph/0603237
- Masso, E., & Toldra, R. 1999, *Phys. Rev. D*, 60, 083503
- R. N. Mohapatra and G. Senjanović, *Phys. Rev. Lett.* **44**, 912 (1980)
- Munyanza, F., & Biermann, P. L. 2005, *A&A*, 436, 805

- Padmanabhan, T. 1993, *Structure formation in the universe*, Cambridge University Press
- Palla, F., Salpeter, E. E. & Stahler, S. W. 1983, *ApJ*, 271, 632
- Peebles, P. J. E. 2001, *ApJ*, 557, 495
- Pontecorvo, B. 1967, *JETP*, 53, 1717
- Riemer-Sørensen, S., Hansen, S. H., & Pedersen, K. 2006, *ApJ*, 644, L33
- Rybicki, G. B., & Lightman, A. P. 1979, *Radiative Processes in Astrophysics* (New York: Wiley)
- Seljak, U., et al. 2005, *Phys. Rev. D*, 71, 103515
- Shapiro, P. R., & Kang, H. 1987, *ApJ*, 318, 32
- Shaposhnikov, M., & Tkachev, I. 2006, [arXiv:hep-ph/0604236](https://arxiv.org/abs/hep-ph/0604236)
- Shi, X. D., & Fuller, G. M. 1999, *Phys. Rev. Lett.*, 82, 2832
- Shull, J. M., & van Steenberg, M. E. 1985, *ApJ*, 298, 268
- Sommer-Larsen, J., & Dolgov, A. D. 2001, *ApJ*, 551, 608
- Sorel, M., Conrad, J. M., & Shaevitz, M. 2004, *Phys. Rev. D*, 70, 073004
- Spergel, D.N., et al. (WMAP) 2003, *ApJS*, 148, 175
- Spergel, D.N., et al. (WMAP) 2006, [arXiv:astro-ph/0603449](https://arxiv.org/abs/astro-ph/0603449)
- Strigari, L. E., Bullock, J. S., Kaplinghat, M., Kravtsov, A. V., Gnedin, O. Y., Abazajian, K., & Klypin, A. A. 2006, [arXiv:astro-ph/0603775](https://arxiv.org/abs/astro-ph/0603775)
- Tegmark, M., Silk, J., Rees, M. J., Blanchard, A., Abel, T. & Palla, F. 1997, *ApJ*, 474, 1
- Viel, M., Lesgourgues, J., Haehnelt, M. G., Matarrese, S., & Riotto, A. 2005, *Phys. Rev. D*, 71, 063534
- Viel, M., Lesgourgues, J., Haehnelt, M. G., Matarrese, S., & Riotto, A. 2006, [arXiv:astro-ph/0605706](https://arxiv.org/abs/astro-ph/0605706)
- Watson, C. R., Beacom, J. F., Yuksel, H. & Walker, T. P. 2006, [arXiv:astro-ph/0605424](https://arxiv.org/abs/astro-ph/0605424)
- Wilkinson, M. I., Kleyna, J. T., Wyn Evans, N., Gilmore, G. F., Read, J. I., Koch, A., Grebel, E. K., & Irwin, M. J. 2006, *EAS Publications Series*, 20, 105

Willman, B., Governato, F., Wadsley, J., & Quinn, T. 2004, MNRAS, 353, 639

Yanagida, T. 1980, Prog. Theor. Phys., 64, 1103

Yoshida, N., Sokasian, A., Hernquist, L., & Springel, V. 2003, ApJ, 591, L1

Zentner, A. R., & Bullock, J. S. 2002, Phys. Rev. D, 66, 043003

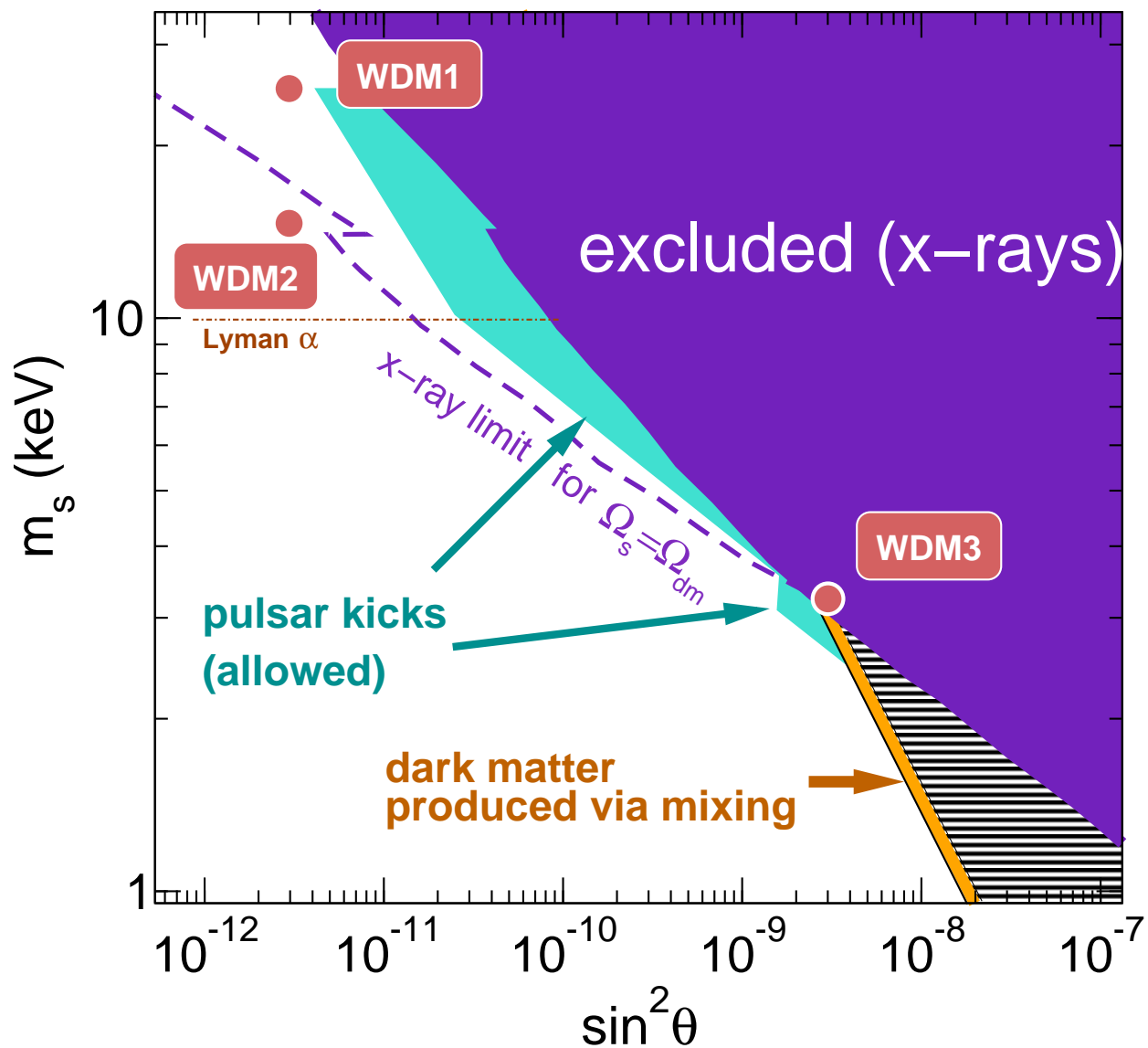


Fig. 1.— The parameter range favored by the pulsar kicks, the current limits from x-ray observations (see text for discussion), and the benchmark points chosen for model calculations.

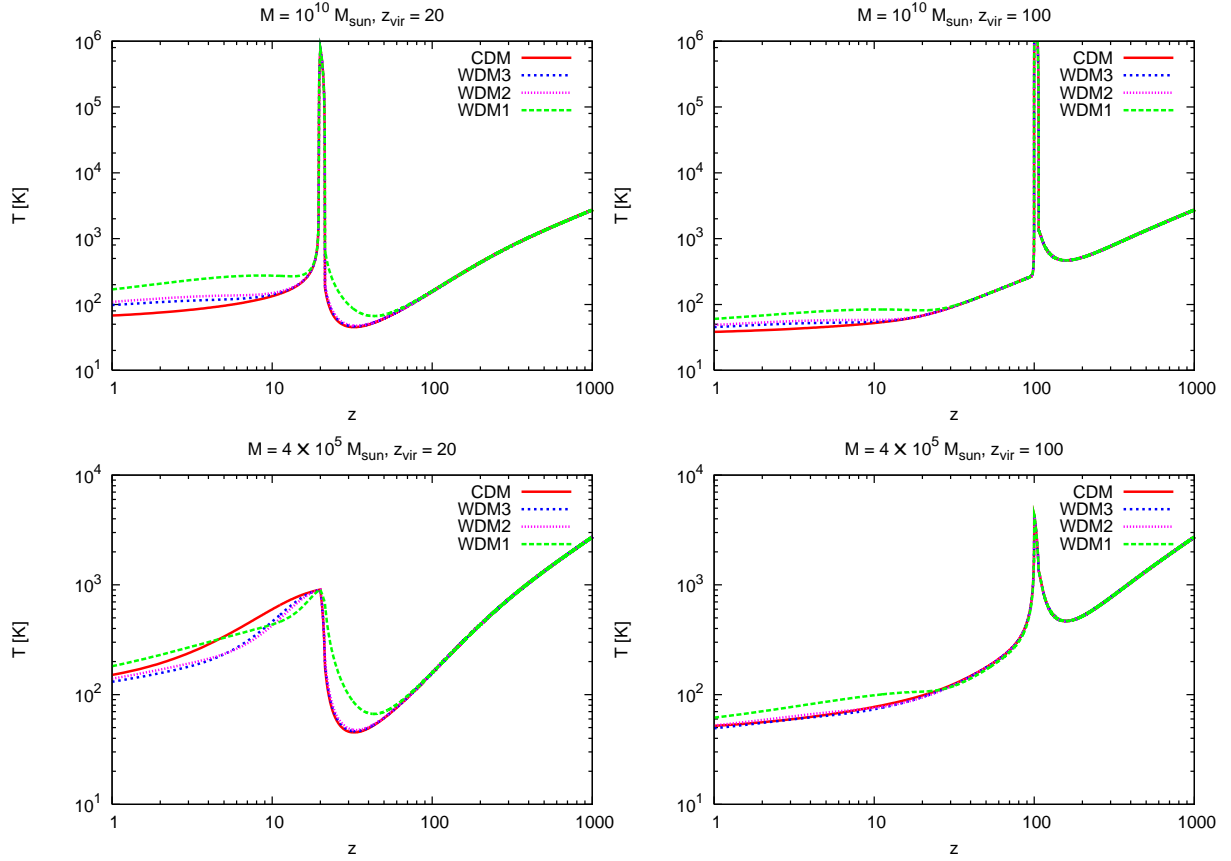


Fig. 2.— Evolution of temperature with redshift for different models: $m_s = 25$ keV and $\sin^2 \theta = 3 \times 10^{-12}$ (WDM1), $m_s = 15$ keV and $\sin^2 \theta = 3 \times 10^{-12}$ (WDM2), $m_s = 3.3$ keV and $\sin^2 \theta = 3 \times 10^{-9}$ (WDM3). M is the cloud mass and z_{vir} is the redshift of virialization.

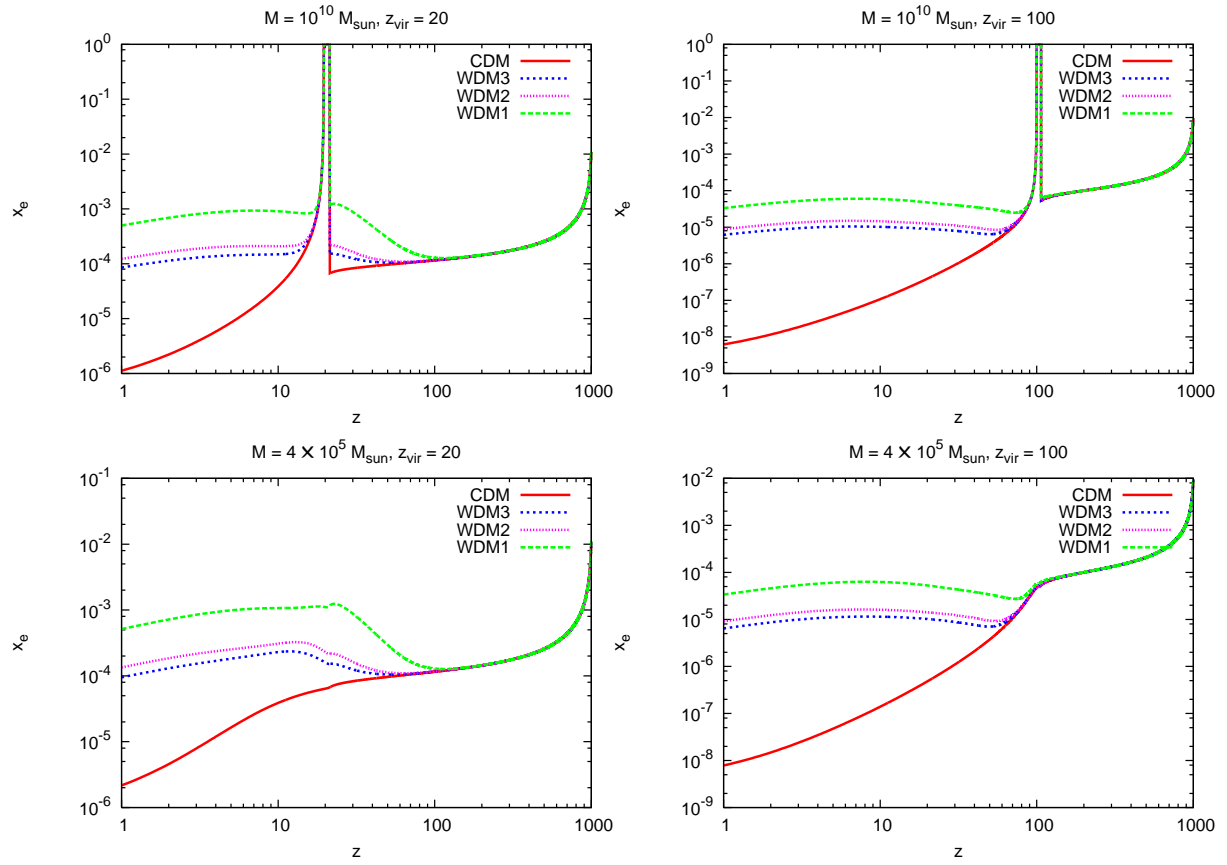


Fig. 3.— The same as in Fig. 2, but for the ionization fraction.

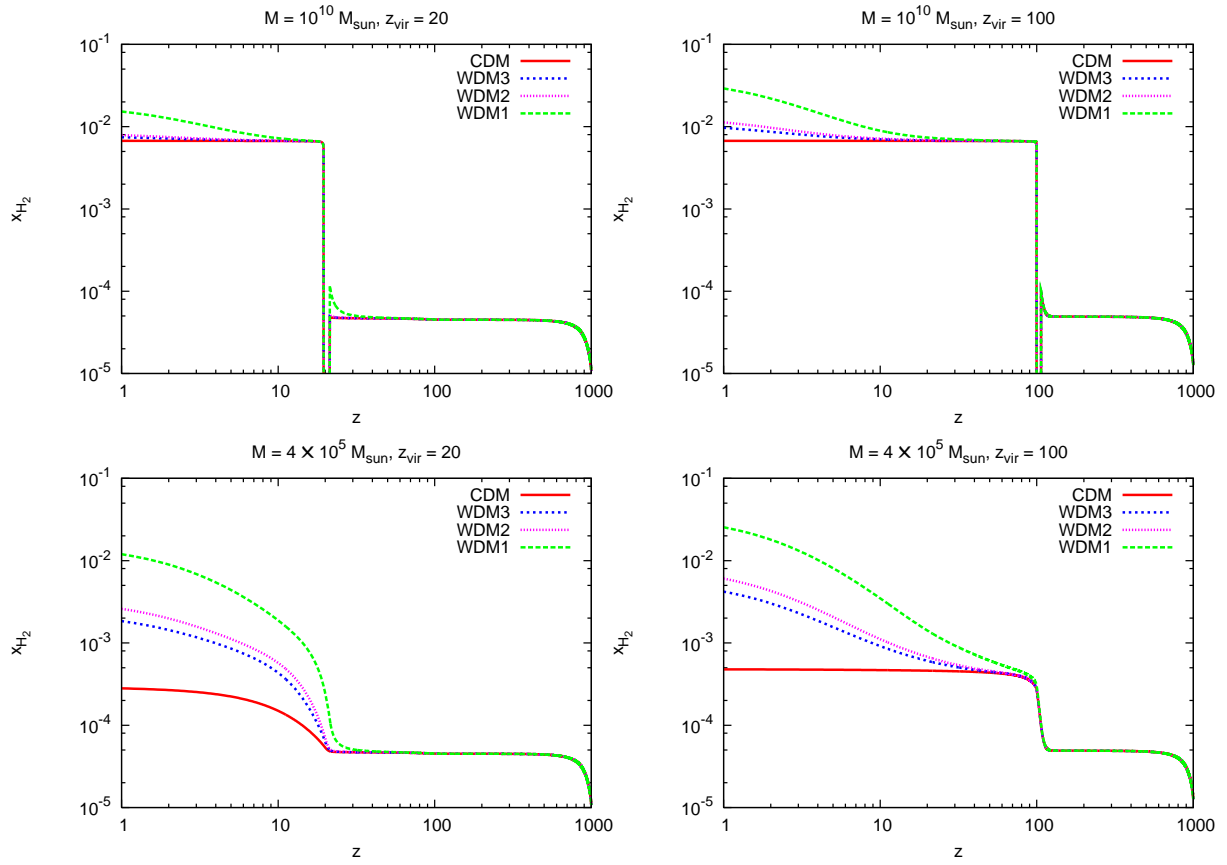


Fig. 4.— The same as in Fig. 2, but for the molecular hydrogen fraction.

Table 1. Reaction rates

Reaction	Rate (cm ³ s ⁻¹ or s ⁻¹)	Reference
H ₂ formation via H ⁻ channel		
$e^- + H \rightarrow H^- + \gamma$	$k_1 = 1.4 \times 10^{-18} T^{0.928} \exp\left(-\frac{T}{16200}\right)$	(Galli & Palla 1998)
$H + H^- \rightarrow H_2 + e^-$	$k_2 = 4.0 \times 10^{-9} T^{-0.17}$	(Galli & Palla 1998)
$H^- + \gamma \rightarrow H + e^-$	$k_3 = 1.1 \times 10^{-1} T_r^{2.13} \exp\left(-\frac{8823}{T_r}\right)$	(Galli & Palla 1998)
H ₂ formation via H ₂ ⁺ channel		
$H^+ + H \rightarrow H_2^+ + \gamma$	$\log k_4 = -19.38 - 1.523 \log T + 1.118 (\log T)^2 - 0.1269 (\log T)^3$	(Galli & Palla 1998)
$H_2^+ + H \rightarrow H_2 + H^+$	$k_5 = 6.4 \times 10^{-10}$	(Galli & Palla 1998)
$H_2^+ + \gamma \rightarrow H + H^+$	$k_6 = 2.0 \times 10^1 T_r^{1.59} \exp\left(-\frac{82000}{T_r}\right)$	(Galli & Palla 1998)
Collisional dissociation of H ₂		
$H_2 + H \rightarrow 3H$	$k_7 = k_{7,H}^{1-a} k_{7,L}^a$ $k_{7,L} = 1.12 \times 10^{-10} \exp\left(-\frac{7.035 \times 10^4}{T}\right)$ $k_{7,H} = 6.5 \times 10^{-7} T^{-1/2} \exp\left(-\frac{\chi_{H_2}}{kT}\right) [1 - \exp\left(-\frac{6000}{T}\right)]$ $a = \left(1 + \frac{n_H}{n_{cr}}\right)^{-1}$ $\log n_{cr} = 4.0 - 0.416 \log T_4 - 0.327 (\log T_4)^2$	(Shapiro & Kang 1987) (Palla, Salpeter & Stahler 1983)
$H_2 + H_2 \rightarrow 2H + H_2$	$k_8 = k_{8,H}^{1-a} k_{8,L}^a$ $k_{8,L} = 1.18 \times 10^{-10} \exp\left(-\frac{6.95 \times 10^4}{T}\right)$ $k_{8,H} = 1.3 \times 10^{-9} \exp\left(-\frac{5.33 \times 10^4}{T}\right)$ $a = \left(1 + \frac{n_{H_2}}{n_{cr}}\right)^{-1}$ $\log n_{cr} = 4.845 - 1.3 \log T_4 + 1.62 (\log T_4)^2$	(Shapiro & Kang 1987) (Shapiro & Kang 1987)
$H_2 + e^- \rightarrow 2H + e^-$	$k_9 = 1.3 \times 10^{-18} T^2 \exp\left(-\frac{\chi_{H_2}}{kT}\right)$	(Lenzuni, Chernoff & Salpeter 1991)
Photo-dissociation of H ₂		
$H_2 + \gamma \rightarrow H_2^* \rightarrow 2H$	$k_{10} = 1.1 \times 10^8 j(\bar{\nu})$ $j(\bar{\nu})$ is the CMB radiation flux in erg cm ⁻² s ⁻¹ at $h\bar{\nu} = 12.87$ eV	(Abel et al. 1997)
$H_2 + \gamma \rightarrow 2H$	$k_{11} = \int_{\nu_{th}^p}^{\infty} 4\pi\sigma_{11}(\nu) \frac{J_\nu}{h\nu} d\nu$ $h\nu_{th}^p = 14.159$ eV, $J_\nu = \frac{2h\nu^3}{c^2} \frac{1}{\exp\left(\frac{h\nu}{kT_r}\right) - 1}$ is the CMB intensity $\sigma_{11}(\nu) = \frac{1}{1+y} \sigma_{11}^p(\nu) + \frac{y}{1+y} \sigma_{11}^o(\nu)$ σ_{11}^p and σ_{11}^o are the crosssections for para- and ortho-H ₂ respectively, $y \approx 3$ is the ortho-, to para-H ₂ ratio	(Abel et al. 1997)
Ionization and recombination of H		
$H + \gamma \rightarrow H^+ + e^-$	$k_{12} = \int_{\nu_{th}^H}^{\infty} 4\pi\sigma_{12}(\nu) \frac{J_\nu}{h\nu} d\nu$ $h\nu_{th}^H = 13.6$ eV $\sigma_{12} = 7.909 \times 10^{-18} \text{ cm}^{-2} \left(\frac{\nu}{\nu_{th}}\right)^{-3}$	(Rybicki & Lightman 1979)
$H^+ + e^- \rightarrow H + \gamma$	$k_{13} = 8.4 \times 10^{-11} T^{-1/2} T_3^{-0.2} \left(1 + T_6^{0.7}\right)^{-1}$	(Galli & Palla 1998)
$H + e^- \rightarrow H^+ + 2e^-$	$k_{14} = 5.85 \times 10^{-11} T^{1/2} \left(1 + T_5^{1/2}\right)^{-1} \exp\left(-\frac{157809.1}{T}\right)$	(Haiman, Thoul & Loeb 1996)

Table 1—Continued

Reaction	Rate ($\text{cm}^3 \text{s}^{-1}$ or s^{-1})	Reference
Ionization of H by the photons from the sterile neutrino decays (Ly α ionization wedge and ionization by the secondary electrons)		
$H + \gamma \rightarrow H^+ + e^-$	see text eq. (B1)	

Note. — The binding energy of H₂ is $\chi_{H_2}/k = 5.197 \times 10^4$ K. T and $T_r = 2.725(1+z)$ are the gas and the CMB temperatures, respectively. J_ν is the CMB intensity. $I_\nu(z)$ is the intensity of the photons from the sterile neutrino decays at redshift z . $T_n = T/10^n$ K. $x_e(z)$, z_{rec} and E_0 are the ionization fraction at redshift z , redshift of recombination and the energy of the photon produced in the sterile neutrino decays.

Table 2. Cooling/heating processes

Cooling/heating function (erg cm ⁻³ s ⁻¹)	Reference
H cooling	
$\Lambda_H(T, T_r) = \Lambda_{H-e}(T) + \Lambda_{rec}(T) + \Lambda_{ioniz}(T) - \Gamma_{PD}(T_r)$	
a) excitation of H by collisions with e ⁻ $\Lambda_{H-e}(T) = 7.5 \times 10^{-19} \left(1 + T_5^{1/2}\right)^{-1} \exp\left(-\frac{118348}{T}\right) n_e n_H$	(Haiman, Thoul & Loeb 1996)
b) recombination to H $\Lambda_{rec}(T) = 1.04 \times 10^{-16} k_{13} n_e n_H^+$	(Haiman, Thoul & Loeb 1996)
c) ionization of H by collisions with e ⁻ $\Lambda_{ioniz}(T) = 2.17 \times 10^{-11} k_{14} n_e n_H$	(Haiman, Thoul & Loeb 1996)
d) photo-ionization of H $\Gamma_{PD}(T_r) = 4\pi n_H \int_{\nu_{th}^H}^{\infty} \sigma_{12}(\nu) \frac{J_\nu}{h\nu} (h\nu - h\nu_{th}^H) d\nu$ $h\nu_{th}^H = 13.6 \text{ eV}$	
H ₂ cooling	
$\Lambda_{H_2}(T, T_r) = \Lambda_{H-H_2}(T, T_r) + \Lambda_{H_2-H_2}(T, T_r) + \Lambda_{form}(T, T_r) + \Lambda_{diss}(T) - \Gamma_{PD1}(T_r) - \Gamma_{PD2}(T_r)$	
a) collisional excitation of H ₂	
i) excitation by collisions with H $\Lambda_{H-H_2}(T) = \frac{\Lambda^H(LTE)\Lambda^H(n \rightarrow 0)}{\Lambda^H(n \rightarrow 0) + \Lambda^H(LTE)} n_{H_2} n_H$	(Galli & Palla 1998)
ii) excitation by collisions with H ₂ $\Lambda_{H_2-H_2}(T) = \left(\frac{\Lambda_r^{H_2}(LTE)\Lambda_r^{H_2}(n \rightarrow 0)}{\Lambda_r^{H_2}(n \rightarrow 0) + \Lambda_r^{H_2}(LTE)} + \frac{\Lambda_v^{H_2}(LTE)\Lambda_v^{H_2}(n \rightarrow 0)}{\Lambda_v^{H_2}(n \rightarrow 0) + \Lambda_v^{H_2}(LTE)} \right) n_{H_2}^2$	(Hollenbach & McKee 1979)
$\Lambda^H(LTE) = \Lambda_r^H(LTE) + \Lambda_v^H(LTE)$	(Hollenbach & McKee 1979)
$\log \Lambda^H(n \rightarrow 0) = -103 + 97.59 \log T - 48.05 (\log T)^2 + 10.8 (\log T)^3 - 0.9032 (\log T)^4$	(Galli & Palla 1998)
$\Lambda_r^{H,H_2}(LTE) = \frac{1}{n_{H,H_2}} \left\{ \left(\frac{9.5 \times 10^{-22} T_3^{3.76}}{1 + 0.12 T_3^2} \right) \exp\left[-\left(\frac{0.13}{T_3}\right)^3\right] + 3 \times 10^{-24} \exp\left(-\frac{0.51}{T_3}\right) \right\}$	(Hollenbach & McKee 1979)
$\Lambda_v^{H,H_2}(LTE) = \frac{1}{n_{H,H_2}} \left[6.7 \times 10^{-19} \exp\left(-\frac{5.86}{T_3}\right) + 1.6 \times 10^{-18} \exp\left(-\frac{11.7}{T_3}\right) \right]$	(Hollenbach & McKee 1979)
$\Lambda_r^{H_2}(n \rightarrow 0) = 0.25 \left[5\gamma_2^{H_2} \exp\left(-\frac{E_{20}^r}{kT}\right) E_{20}^r + 0.75 \left[\frac{7}{3} \gamma_3^{H_2} \exp\left(-\left(\frac{E_{31}^r}{kT}\right)\right) E_{31}^r \right] \right]$	(Hollenbach & McKee 1979)
$\Lambda_v^{H_2}(n \rightarrow 0) = 1.4 \times 10^{-12} T^{1/2} \exp\left(-\frac{12000}{T+1200}\right) \exp\left(-\frac{E_{10}^v}{kT}\right) E_{10}^v$	(Hollenbach & McKee 1979)
$\gamma_J^{H_2} = (3.3 \times 10^{-12} + 6.6 \times 10^{-12} T_3) \left\{ 0.276 J^2 \exp\left[-\left(\frac{J}{3.18}\right)^{1.7}\right] \right\}$	(Hollenbach & McKee 1979)
$\frac{3}{5} E_{31}^r/k = E_{20}^r/k = 512 \text{ K}, E_{10}^v/k = 5860 \text{ K}$	(Hollenbach & McKee 1979)
b) H ₂ formation cooling $\Lambda_{form}(T) = 1.6022 \times 10^{-12} \left(3.53 \frac{k_1 k_2}{k_2 + k_3/n_H} + 1.83 \frac{k_4 k_5}{k_5 + k_6/n_H} \right) \left[1 - \left(1 + \frac{n_{cr}}{n}\right)^{-1} \right] n_H n_e$ $n_{cr} = 10^6 T^{-1/2} / \left\{ 1.6 x_H \exp\left[-\left(\frac{400}{T}\right)^2\right] + 1.4 x_{H_2} \exp\left[-\frac{12000}{T+1200}\right] \right\}$	(Shapiro & Kang 1987) (Hollenbach & McKee 1979)
c) collisional dissociation of H ₂ $\Lambda_{diss}(T) = 7.17145 \times 10^{-12} (n_H k_7 + n_{H_2} k_8 + n_e k_9) n_{H_2}$	(Shapiro & Kang 1987)

Table 2—Continued

Cooling/heating function (erg cm ⁻³ s ⁻¹)	Reference
d) photo-dissociation of H ₂	
i) H ₂ + γ → H ₂ [*] → 2H $\Gamma_{PD1}(T_r) = 6.4 \times 10^{-13} k_{10} n_{H_2}$	(Abel et al. 1997)
ii) H ₂ + γ → 2H $\Gamma_{PD2}(T_r) = 4\pi n_{H_2} \left[\frac{1}{y+1} \int_{\nu_{th}^p}^{\infty} \sigma_{11}^p(\nu) \frac{J_\nu}{h\nu} (h\nu - h\nu_{th}^p) d\nu + \frac{y}{y+1} \int_{\nu_{th}^o}^{\infty} \sigma_{11}^o(\nu) \frac{J_\nu}{h\nu} (h\nu - h\nu_{th}^o) d\nu \right]$ $h\nu_{th}^p = 14.159$ eV, $h\nu_{th}^o = 14.675$ eV, $y = 3$ is the ortho-H ₂ to para-H ₂ ratio	(Abel et al. 1997)
Compton cooling	
$\Lambda_{comp}(T, T_r) = 1.017 \times 10^{-37} T_r^4 (T - T_r) n_e$	(Haiman, Thoul & Loeb 1996)
bremsstrahlung	
$\Lambda_{brem}(T, T_r) = \Lambda_{brem}(T) - \Lambda_{brem}(T_r)$	
$\Lambda_{brem}(T) = 1.42 \times 10^{-27} g_{ff} T^{1/2} n_e n_{H^+}$ $g_{ff} = 1.1 + 0.34 \exp \left[- (5.5 - \log T)^2 / 3 \right]$	(Haiman, Thoul & Loeb 1996)
heating due to the photons from the sterile neutrino decays	
$\Lambda_s(z) = -\Gamma_s(z)$	
see text eq. (B2)	

Note. — T and $T_r = 2.725(1+z)$ are the gas and CMB temperature respectively. J_ν is the CMB intensity. $I_\nu(z)$ is the intensity of the photons from the sterile neutrino decays at redshift z . $T_n = T/10^n$ K. $\sigma_i(\nu)$ and k_i are given in the table 1. $x_e(z)$, z_{rec} and E_0 are the ionization fraction at redshift z , redshift of recombination and the energy of the photon produced in the sterile neutrino decays.